Sensors & Diagnostics

PAPER

View Article Online
View Journal | View Issue

Cite this: *Sens. Diagn.*, 2022, **1**, 1224

An ESIPT-based fluorescent probe for the detection of multiple analytes and a facile approach to discriminate between arsenate and pyrophosphate in water†

Srushti Gadiyaram, Vikas D. Ghule, Amrita Ghosh and D. Amilan Jose *

A simple ESIPT-based fluorescent probe for the detection of the multiple analytes such as chromium (Cr^{3+}), arsenate ($HAsO_4^{2-}$), and pyrophosphate (PPi, $P_2O_7^{4-}$) has been reported. The probe **HJ-DNP** displayed weak emission in organic solvents owing to excited-state intramolecular proton transfer (ESIPT) and –C═N isomerization. However, upon the addition of water, the fluorescence emission could be increased to a maximum through the aggregation-induced emission (AIE) behavior of **HJ-DNP**. The combined effects of ESIPT and AIE in the DMSO–water mixture were used to sense multiple analytes. The probe **HJ-DNP** could selectively detect Cr^{3+} through the CHEF mechanism with a turn-on fluorescence response. The limit of detection (LOD) for Cr^{3+} ions was estimated to be as low as 3.9 μM. The probe **HJ-DNP** was also used to detect Cr^{3+} ions in tomato extract. The probe **HJ-DNP** also binds preferentially with arsenate and pyrophosphate (PPi) in the presence of various anions. The sensing of arsenate and PPi could be carried out through naked-eye detection with a color change from orange to red; the LOD values are calculated to be 3.9 μM and 0.19 mM for arsenate and PPi, respectively. It was found that arsenate detection is more sensitive than PPi detection. Moreover, the different emission behavior of **HJ-DNP** in the presence of arsenate or PPi was used to easily discriminate them. The probe **HJ-DNP** was used to detect arsenate in real water samples. Arsenate was also detected and adsorbed from water samples using **HJ-DNP** incorporating alginate polymer beads.

Received 1st September 2022,
Accepted 13th September 2022

DOI: 10.1039/d2sd00157h

rsc.li/sensors

1. Introduction

Fluorescence-based sensors of anions and cations are of great interest to researchers due to their high sensitivity and fluorescence bio-imaging abilities.[1–4] Several fluorescent chemical sensors, working on the principles of photoinduced electron transfer (PET), internal charge transfer (ICT), chelation-enhanced fluorescence (CHEF), excited-state intramolecular proton transfer (ESIPT), aggregation-induced emission (AIE), and aggregation-induced quenching (AIQ), are known for a variety of anions and cations that are biologically and environmentally relevant.[5]

Aggregation-induced emission (AIE) is a photophysical phenomenon associated with chromophore aggregation.[6,7] In the AIE process, non-emissive luminogens are induced to emit *via* aggregate formation.[8] In general, a molecule can exhibit ESIPT fluorescence if its structure incorporates an intramolecular hydrogen bonding interaction between –OH/NH_2 hydrogen bond donor and a hydrogen bond acceptor (═N– and –C═O).[9] ESIPT fluorescence probes have the advantage of showing very significant Stokes shifts. Generally, ESIPT-based fluorescent probes are designed in a way in which the H-bond is initially blocked, inhibiting the ESIPT process; consequently, only enol emission is possible.[10] However, exposure to a specific analyte can allow a H-bond and the keto form, unlocking the ESIPT process.

Most AIE- and ESIPT-based fluorescent sensors are known to detect either one individual analyte or they act as dual-responsive probes for two analytes, rather than sensing multiple analytes in parallel.[11] Dual-responsive probes contain a distinct sensing group for each analyte.[12] Therefore, developing an ESIPT-based multi-analyte chemosensor is crucial for environmental and biological applications.[13–17] Different interaction modes need to be considered to design a multianalyte probe, which increases the design difficulty. From a practical point of view, designing such molecular probes with differential responses towards multiple analytes is cost-effective and highly desirable. They can detect more than one analyte based on creating different output signal responses to different analytes.

Department of Chemistry, National Institute of Technology (NIT) Kurukshetra, Kurukshetra – 136119, Haryana, India. E-mail: amilanjosenit@nitkkr.ac.in

† Electronic supplementary information (ESI) availabl. See DOI: https://doi.org/10.1039/d2sd00157h

Cr^{3+} is a heavy metal ion and a nutrient necessary for balancing human and animal diets. However, excessive consumption of Cr^{3+} is known to negatively affect human health. Thus, the selective and sensitive detection of Cr^{3+} ions in environmental and biological samples is required.[18,19] Although many chemical sensors for Cr^{3+} have been designed, most of them are unsuccessful in detecting Cr^{3+} ions in an aqueous medium, making them unsuitable for practical applications.[20–29] Therefore, it is essential to design new water-friendly chemical sensors for the sensitive detection of Cr^{3+}.

Phosphorus- and arsenic-derived oxyanions exhibit similar properties, notably inorganic phosphate (Pi) and arsenate. Their physiochemical similarities make them difficult to differentiate when they co-exist in water.[30] Arsenate is considered to be highly toxic to humans compared with phosphates. Arsenate is also a critical chemical pollutant in water. Several fluorescent chemical sensors related to the detection of phosphates are known but reports of fluorescent chemical sensors for arsenate are rare.[31,32] Therefore, the development of new, simple, sensitive, and reliable fluorescence-based methods for arsenate ion recognition is highly desired.

In this work, a multianalyte-responsive probe, **HJ-DNP**, was developed *via* conjugating 8-hydroxyjulolidine-9-carboxaldehyde and 2,4-dinitrophenylhydrazine through a Schiff base reaction (Scheme 1). The probe **HJ-DNP** displayed aggregation-induced emission (AIE) behaviour in a DMSO–water mixture. The probe **HJ-DNP** was also studied for the fluorescent detection of Cr^{3+} and discrimination between PPi and arsenate in aqueous solution.

2. Results and discussion

The probe **HJ-DNP** was prepared *via* a condensation reaction between 8-hydroxyjulolidine-9-carboxaldehyde and 2,4-dinitrophenyl hydrazine in a single-step reaction (Scheme 1). The compound **HJ-DNP** was isolated in pure form with 80% yield, and the characterization data matched well with the desired product (see the experimental details below and ESI† Fig. S1–S3).

2.1. Photophysical and water-dependent aggregation studies

The UV-vis spectrum of **HJ-DNP** (0.05 mM) in dimethyl sulphoxide (DMSO) displayed two peaks at 365 nm (ε = 12 400 M^{-1} cm^{-1}) and 470 nm (ε = 7240 M^{-1} cm^{-1}). The fluorescence emission spectrum of **HJ-DNP** in DMSO exhibits weak broad emission at 420 nm and 585 nm upon excitation at 365 nm (Fig. S4†). Almost all solvents result in weak fluorescence emission (Fig. S5†). The large Stokes shift of around 585 nm was assigned to proton-transfer tautomer emission. The weak emission of **HJ-DNP** is owing to the excited-state intramolecular proton-transfer (ESIPT) process (the phenolic proton transfers to the imine nitrogen atom) and C=N isomerization.[33]

The photosensitivity of the probe **HJ-DNP** was explored, as it has two nitro groups that are sensitive to UV exposure. This implies that under strong UV light irradiation, the probe can be degraded. To avoid such a situation, the experiments were performed with fresh stock solutions and were carried out mostly *via* avoiding direct contact with UV light. Experiments were monitored for up to 90 min (Fig. S6†).

The formation of an intramolecular hydrogen bond between hydrogen-donor and hydrogen-acceptor groups is a prerequisite for ESIPT. The compound **HJ-DNP** bears a 2,4-dinitrophenylhydrazine N atom as a proton acceptor and a julolidine hydroxyl group as the proton donor.

To confirm the ESIPT process in **HJ-DNP**, the ground state (S_0) and first excited-state (S_1) energies for both the enol and keto tautomer forms of **HJ-DNP** were calculated using the respective optimized geometries (Fig. 1a). The molecular geometries of the receptor keto–enol tautomer and the transition state have been optimized using the B3LYP/6-311G(d,p) level of theory and are shown in Fig. 1b. A transition state *via* direct H-transfer bonding between the oxygen atom (–OH) and the azomethine (C=N) nitrogen

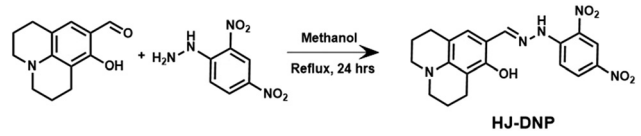

Scheme 1 A schematic representation of the synthesis of **HJ-DNP**.

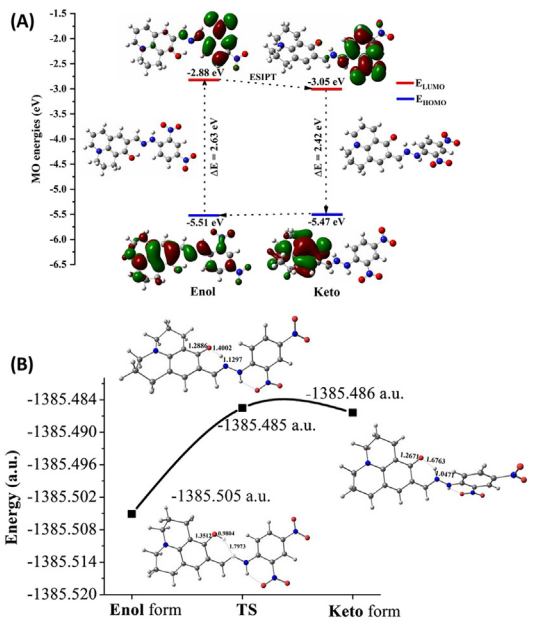

Fig. 1 (a) The optimised keto–enol molecular geometries of the probe **HJ-DNP** using the B3LYP/6-311G(d,p) level of theory. (b) The keto–enol tautomer and transition-state energy levels of **HJ-DNP**.

atom (see Fig. 1) was determined. The C═O, O···H, and H–N bond distances in the keto form are 1.2671, 1.6763, and 1.0471 Å, respectively. In the enol form, the C–O, O–H, and H···N distances are 1.3512, 0.9804, and 1.7973 Å, respectively. As can be seen, strong H-bonding exists in the tautomer, and H-transfer from O to N is established. In the transition state, the C–O, N–H, and O–H distances increase, indicating proton transfer. The C–O, O···H, and H···N distances in the transition state are 1.2886, 1.4002, and 1.1297 Å, respectively.

The HOMO–LUMO energy difference was reduced from 2.63 eV for the enol form to 2.42 eV for the keto form. This observation indicates that the probe **HJ-DNP** undergoes ESIPT. Consequently, the tautomer forms in the excited state, which is responsible for the emission properties.

The probe **HJ-DNP** shows enhancement in emission at 585 nm with an increasing amount of water in a DMSO mix (Fig. 2). The intensity of the emission peak at *ca.* 585 nm increased continuously, showing a ten-fold increase with 90% water in DMSO (v/v) compared with 0% water. Up to 60% water, almost no change in emission was obtained, but emission enhancement was observed beyond that. The enhancement of emission in the presence of water was due to the formation of aggregates and AIE. It is already known from the literature that ESIPT and AIE occur in hydroxy aromatic imines, and the emission is dependent on the proportion of water in the solvent.[34–37]

Therefore, it is proposed that the red emission that occurred at 585 nm upon the addition of water is due to a combined effect of ESIPT and AIE. Further, to confirm the formation of aggregates in the presence of water, the particle size of **HJ-DNP** was studied *via* the dynamic light scattering (DLS) method in DMSO and a DMSO–water mixture (Fig. S8†). The average particle size of **HJ-DNP** in the DMSO–water mixture increased to 1268 nm compared to 232 nm in DMSO alone. The results suggest that the compound **HJ-DNP** tends to form aggregates in DMSO–water. Further, it validates the tendency of **HJ-DNP** to show aggregation-induced emission (AIE) behaviour (Scheme 2).

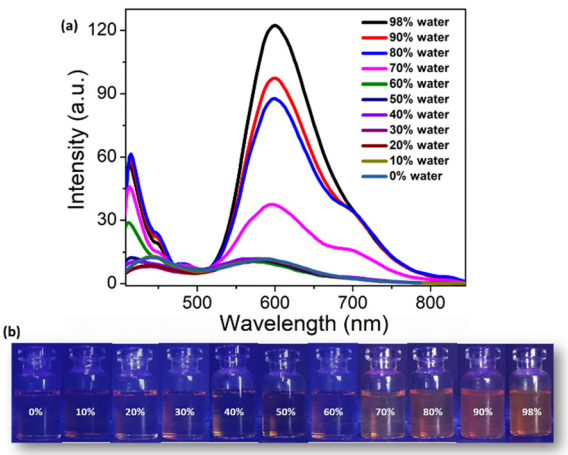

Fig. 2 (a) The emission spectra from aggregation studies of the probe **HJ-DNP** (0.1 mM) in DMSO with different amounts of water and (b) visual representation of aggregation-induced emission (AIE) upon exposure to UV light.

2.2. Chromium-ion selectivity

The binding properties of **HJ-DNP** towards different transition-metal and heavy-metal ions, such as Ni^{2+}, Ag^{+}, Fe^{2+}, Fe^{3+}, Cr^{3+}, Cd^{2+}, Cu^{2+}, Mn^{2+}, Na^{+}, Mg^{2+}, Ca^{2+}, Co^{2+}, and Hg^{2+}, were investigated by fluorescence experiments. All the experiments were carried out in a DMSO–water (80 : 20) mixture, where weak monomer emission was predominant. The fluorescence emission spectra of **HJ-DNP** (0.1 mM) with excess amounts (5 equivalents, 0.5 mM) of different metal ions were measured. A considerable enhancement in emission was observed at 420 nm (λ_{ex} = 365 nm) along with a decrease in emission at 585 nm only in the presence of Cr^{3+}. This enhancement (at 420 nm) was not found in the case of any other metals (Fig. 3a). Systematic emission titration was used to determine the sensitivity of Cr^{3+} binding with **HJ-DNP**. As shown in Fig. 3b, with the addition of Cr^{3+}, emission at 585 nm continuously decreased and an increase in the emission peak at 420 nm was observed, with a clear isosbestic point at 540 nm. The binding constant for Cr^{3+} was calculated to be 4.81×10^{4} M^{-1}. The limit of detection (LOD) was estimated to be 3.9×10^{-6} M. 1 : 1 stoichiometric binding between **HJ-DNP** and Cr^{3+} was established based on a Job plot (Fig. S9†).

The increase in the fluorescence intensity at 420 nm and the decrease at 585 nm in the presence of Cr^{3+} ions may be due to the inhibition of H-bonding; therefore, the ESIPT process was blocked (Scheme 3). The observed emission at 420 nm in the DMSO–water (80 : 20) mixture corresponds to the standard form of **HJ-DNP**. In contrast, emission at 585 nm arises due to intramolecular H-bonding between the julolidine OH group and the hydrazine N atom of **HJ-DNP**. When a Cr^{3+} ion binds with the julolidine OH group and the hydrazine N atom of **HJ-DNP**, it does not allow the ESIPT process (Scheme 3) and the emission at 420 nm is recovered.

Further, the Cr^{3+} ion binding behaviour of **HJ-DNP** was also tested *via* UV-vis experiments. The systematic titration of **HJ-DNP** (0.05 mM) with Cr^{3+} (0–0.145 mM) showed a decrease in absorbance at 470 nm and a shift in the absorbance maximum from 365 nm to 340 nm (Fig. S10†). Based on the absorbance titration studies, the binding constant (K_a) was calculated to be 4.34×10^{4} M^{-1}, closely matching the value

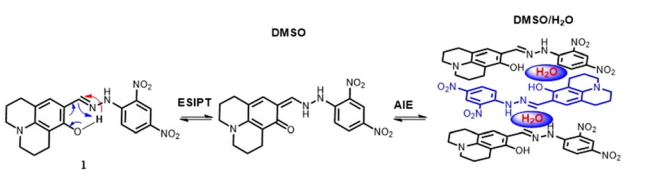

Scheme 2 The proposed ESIPT mechanism and the AIE behaviour of the probe **HJ-DNP**.

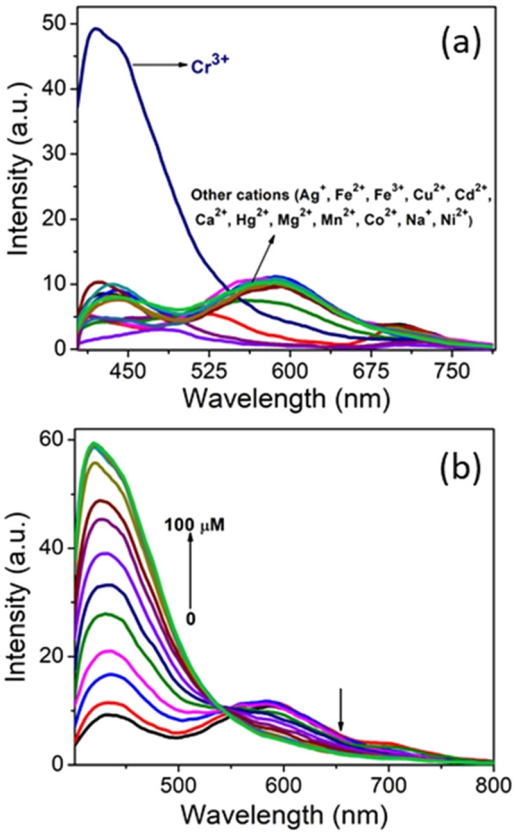

Fig. 3 (a) The emission spectra of the probe **HJ-DNP** (0.1 mM) in the presence of different metal ions, such as Ni^{2+}, Ag^{+}, Fe^{2+}, Fe^{3+}, Cr^{3+}, Cd^{2+}, Cu^{2+}, Mn^{2+}, Na^{+}, Mg^{2+}, Ca^{2+}, Co^{2+}, and Hg^{2+} (0.5 mM). (b) The sensitivity of the probe **HJ-DNP** toward various concentrations of Cr^{3+} (0–100 μM) (λ_{ex} = 365 nm, slit width: 20/20).

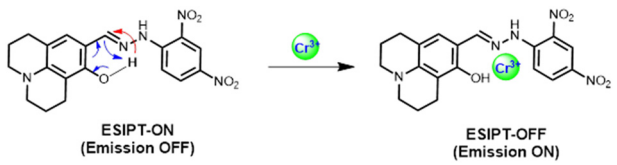

Scheme 3 The proposed mechanism of the interaction of the probe **HJ-DNP** with Cr^{3+}.

obtained from emission titration experiments. Time-resolved fluorescence lifetime measurements were also performed to confirm the turn-on sensor response of **HJ-DNP** in the presence of Cr^{3+}. The average fluorescence lifetime of the probe **HJ-DNP** in the absence of analyte was measured to be 0.82 ns. However, in the presence of Cr^{3+}, it was increased to 2.07 ns (Fig. S11†). The emission quantum yield (Φ) calculated for **HJ-DNP** (Φ = 0.00031) was increased almost three-fold in the presence of Cr^{3+} (Φ = 0.00081) ions.

The proposed binding mode of **HJ-DNP** with Cr^{3+} is shown in Scheme 3. It can be presumed that the chelating mode of **HJ-DNP** binding to Cr^{3+} restricts the molecule, which extends the π-electron conjugation throughout the molecule. The extension in conjugation triggers a switch-ON response in the fluorescence spectrum *via* a chelation-enhanced fluorescence (CHEF) mechanism. The sensing mechanism of the probe toward Cr^{3+} is also confirmed with ESI-mass analysis. As shown in mass experiments, in the presence of Cr^{3+}, the probe displayed a peak at an *m*/*z* value of 449.24 for a 1 : 1 complex of Cr^{3+} with **HJ-DNP**, and the $[2M + H]^{+}$ peak is also observed at an *m*/*z* value of 898.5608. If the analyte is prone to complex formation or is highly concentrated, $[2M + H]^{+}$ ions could also be observed in the full mass spectrum (Fig. S12†).

To gain more insight into the sensing behaviour of **HJ-DNP** toward Cr^{3+}, DFT calculations were carried out using the Gaussian 09 program package. The geometries of **HJ-DNP** and **HJ-DNP** with Cr^{3+} were fully optimized and investigated using the density functional theory method (B3LYP) with the 6-311g(d,p) and LANL2DZ basis sets. The HOMO, LUMO, and bandgap energy values were calculated using DFT studies. The optimized structures of the probe **HJ-DNP** and the corresponding Cr^{3+} adduct are shown in Fig. 4.

The HOMO is delocalized over the whole molecule, while the LUMO is mainly delocalized on 2,4-dinitrophenylhydrazine. In the **HJ-DNP**–Cr^{3+} complex, the HOMO is delocalized over the whole molecule, whereas the LUMO is strongly delocalized on (2,4-dinitrophenyl)hydrazine and slightly on the Cr^{3+} part. The calculated data show that the **HJ-DNP**–Cr^{3+} complex has significantly reduced HOMO energy (−3.9 eV) compared to **HJ-DNP**. The computed energy gaps for the **HJ-DNP** and **HJ-DNP**–Cr^{3+} complexes are 2.76 and 0.85 eV, suggesting that the binding of Cr^{3+} significantly reduces the energy gap and favours an electron transition. The lowering of the HOMO–LUMO energy gap in the **HJ-DNP**–Cr^{3+} complex compared to free **HJ-DNP** probably causes a slight red shift in the emission spectrum of **HJ-DNP** at 420 nm when Cr^{3+} is added. The substantial decrease in the total

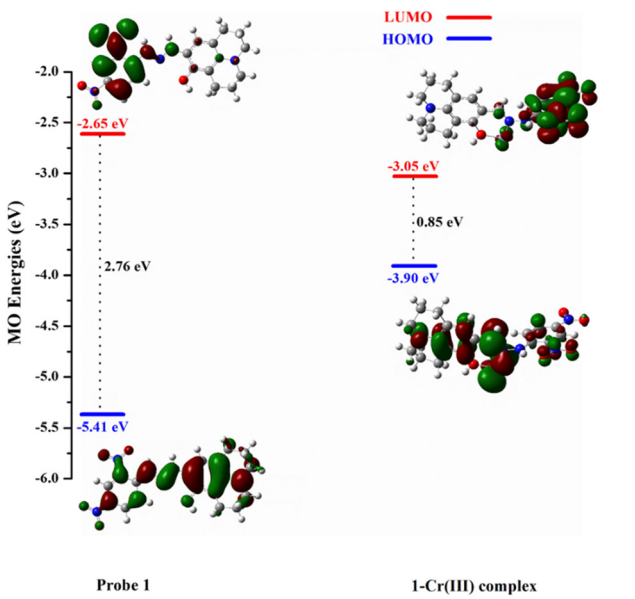

Fig. 4 The optimized structures of the probe **HJ-DNP** and the **HJ-DNP**–Cr^{3+} complex obtained using DFT theory at the B3LYP level with the 6-311g(d,p) and LANL2DZ basis sets.

energy of **HJ-DNP** upon complexation with Cr^{3+} suggests that the **HJ-DNP**–Cr^{3+} complex is highly stable, probably initiating the spectral outcome through the CHEF mechanism.

2.3. Chromium detection in real-life samples

Although chromium(III) ions are an essential element in the human body, excess intake can harm the stomach and blood glucose levels. Recent studies showed that compounds containing Cr^{3+} probably provoke toxicity, leading to carcinogenicity.[38,39]

Vegetables are essential components of the human diet, but studies have demonstrated the presence of trace metals within them. Vegetables grown in heavily polluted water may show heavy-metal contamination.[40]

These metals cannot be removed by washing the vegetables or cooking, even at high temperatures. Hence, we have explored the possible detection of Cr^{3+} in tomatoes (*Solanum lycopersicon*) using the probe **HJ-DNP**. Several studies have described the toxic effects of Cr^{3+} in tomatoes and other plants.[41] Chromium detection experiments were performed with tomato extract spiked with known concentrations of Cr^{3+} (see the ESI†). **HJ-DNP** emission spectra were recorded from Cr^{3+}-spiked tomato extract. As shown in Fig. 5, good linearity (R^2 = 0.982) was observed in a plot of the concentration of Cr^{3+} in tomato extract and the emission intensity at 420 nm. This also provided a LOD of 22.4 nm. Therefore, the probe **HJ-DNP** can be used to detect and quantify Cr^{3+} ions in tomatoes. This could prove to be a powerful tool to quantify an unknown amount of Cr^{3+} in various food samples.

2.4. Binding studies with anions

The binding abilities of **HJ-DNP** with various anions are also monitored *via* UV-vis and fluorescence spectrophotometry. As shown in Fig. 6, in the presence of excess anions (10 equivalents), only PPi and arsenate[42] induced distinct spectral and colour changes. Other relevant anions, such as F^-, PO_4^{3-}, AcO^-, Cl^-, Br^-, I^-, NO_3^-, $H_2PO_4^-$, and HSO_4^-, did not show any noticeable changes in terms of their UV–vis and fluorescence spectra (Fig. 6). The probe **HJ-DNP** immediately changed from dark yellow to red in the presence of PPi and arsenate (Fig. 6a). Anions such as S^{2-}, HS^-, CN^-, CO_3^{2-}, and HCO_3^- also showed definite changes in terms of their UV-vis absorbance. However, the changes are mainly due to deprotonation of the –OH moiety in **HJ-DNP**. As the probe is sensitive to basic pH, these highly basic anions drive the probe **HJ-DNP** to be deprotonated (Fig. S13†).

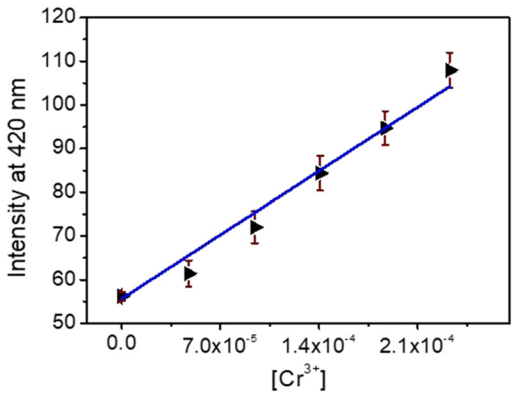

Fig. 5 A plot of the linear relationship between the emission intensity of **HJ-DNP** and the concentration of Cr^{3+} in tomato extract.

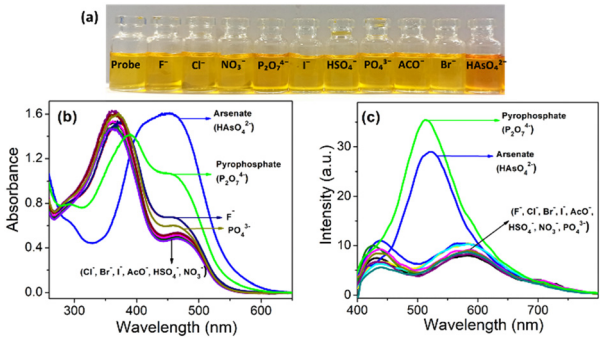

Fig. 6 (a) The visual colour changes of **HJ-DNP** in the presence of different anions. (b) UV-vis absorbance and (c) emission spectra from selectivity studies of the probe **HJ-DNP** (0.1 mM) in the presence of anions such as F^-, PO_4^{3-}, $P_2O_7^{4-}$, CH_3COO^-, Cl^-, Br^-, I^-, NO_3^-, $H_2PO_4^-$, HSO_4^-, and arsenate (10 equivalents).

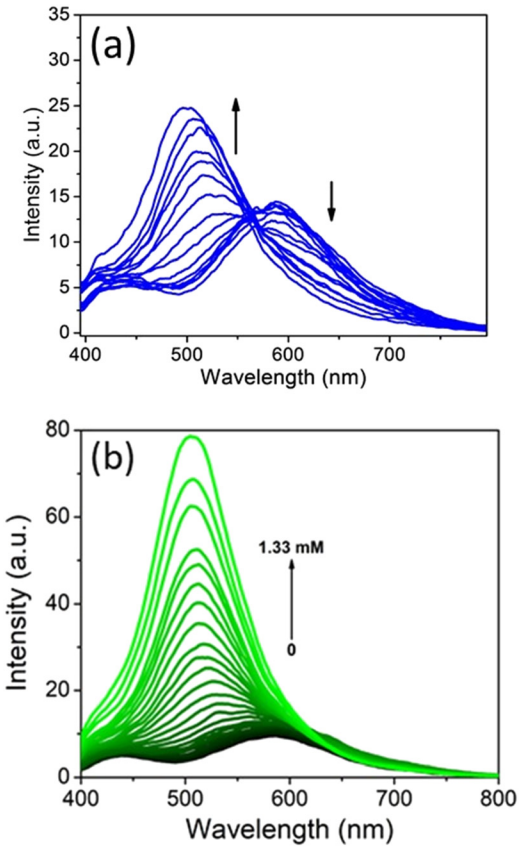

Fig. 7 The emission spectra of the probe **HJ-DNP** (0.1 mM) with various concentrations of (a) arsenate (0–1.17 mM) and (b) PPi ($P_2O_7^{4-}$) (0–1.33 mM) ions (λ_{ex} = 365 nm, slit width: 20/20).

The sensitivity of the probe **HJ-DNP** toward arsenate and PPi was calculated based on systematic titration studies. As shown in Fig. 7a, a decrease in the emission band at 585 nm and an increase in the emission band at 510 nm were observed upon adding arsenate ions to **HJ-DNP**. The stoichiometry of **HJ-DNP** binding with arsenate was calculated through a Job's plot, and the results confirmed the formation of a 1 : 2 (anion : ligand) complex (Fig. S14†). In the UV-vis spectrum, with an increase in the arsenate concentration, a decrease in the absorbance band at 365 nm and a simultaneous increase at 410 nm were observed (Fig. S15†).

The binding constant (4.81×10^4 M^{-1}) and LOD (3.9 μM) values were calculated for arsenate detection *via* the emission method.[43–45] Further, the sensitivity of **HJ-DNP** toward PPi was also determined *via* systematic fluorescence and UV-vis absorbance titration. As shown in Fig. 7b, upon the addition of PPi, the emission band intensity at 505 nm was increased. In the UV-vis spectra, the sensor **HJ-DNP** exhibited ratiometric changes when detecting PPi at 340 nm and 425 nm (Fig. S16†). A Job plot confirmed the 1 : 2 (PPi : **HJ-DNP**) stoichiometry of **HJ-DNP** binding with PPi (Fig. S17†). The LOD and K_a values for PPi were calculated to be 0.19 mM and 8.77×10^2 M^{-1}, respectively. These values revealed that the binding of PPi is very weak and less sensitive compared to arsenate. The sensitivity of arsenate binding is 55 times higher than that of PPi binding.

Furthermore, time-resolved fluorescence lifetime measurements were performed to reconfirm the turn-on sensor responses of **HJ-DNP** towards PPi and arsenate ions. It was observed that the fluorescence decay constants (s) of **HJ-DNP** were affected, as summarized in Table S2.† The average lifetime values of **HJ-DNP** increased to 1.77 ns and 3.24 ns, respectively, for arsenate and PPi (Fig. 8). The relative quantum yield values calculated for **HJ-DNP** with PPi (Φ = 0.0022) and arsenate (Φ = 0.0012) are more than five times that of **HJ-DNP** (Φ = 0.00031), which confirms the turn-on fluorescence response toward PPi and arsenate ions.

Phosphorus- and arsenic-derived oxyanions display similar properties, making them difficult to distinguish when they co-exist. Interestingly, the natures of the emission spectrum changes toward PPi and arsenate are different (Fig. 7), making PPi and arsenate distinguishable.[46–48] PPi displayed emission enhancement at 543 nm, whereas arsenate showed ratiometric changes in emission and enhancement at 523 nm. This spectral difference can be used to identify and discriminate between PPi and arsenate in solution easily. The acidic protons of the probe **HJ-DNP** are involved in binding with the –OH groups of arsenate and pyrophosphate ions, as shown in the proposed mechanism (ESI† Scheme S1).

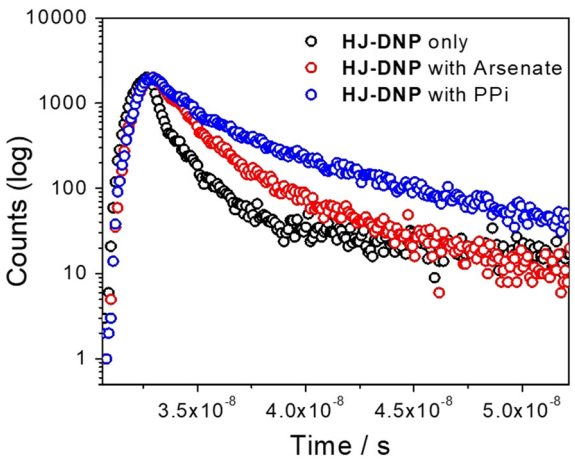

Fig. 8 Lifetime measurements of the probe **HJ-DNP** (0.1 mM) with arsenate (1 mM) and PPi (9.45 mM) in DMSO–water (80 : 20).

FTIR analysis was performed to understand the binding modes of PPi and arsenate. **HJ-DNP** was mixed with different concentrations of PPi and arsenate. These solutions were evaporated, and the solid product was analysed *via* FT-IR using the KBr method. The IR spectra of **HJ-DNP** with and without PPi and arsenate were compared. The IR spectrum of **HJ-DNP** shows a strong band observed at 1604 cm^{-1}, which can be assigned to the stretching vibrations of the –NH group, and the moderately intense bands observed around 2985–3005 cm^{-1} are due to azomethine (–CH=N) stretching. The shifts in the IR bands of –NH, –CH=N, and –OH in the presence of PPi and arsenate confirm the involvement of these groups during the binding process (Fig. S18†).

Further, ^{1}H-NMR spectra of **HJ-DNP** were also obtained in the presence of arsenate and PPi to confirm the binding mode of **HJ-DNP** with these anions. The interaction of PPi and arsenate caused significant changes in the chemical shifts in the ^{1}H-NMR spectra of **HJ-DNP**. The protons of –OH (15.3 ppm) and –NH (9.9 ppm) disappeared due to hydrogen bonding between PPi/arsenate and **HJ-DNP**. ^{1}H-NMR experiments confirm the involvement of –OH and –NH groups in binding with arsenate (Fig. S19†). Based on IR and ^{1}H-NMR analysis, the mechanism of the binding of PPi and arsenate with **HJ-DNP** is proposed in ESI† Scheme S1.

The binding behaviour of **HJ-DNP** with arsenate and PPi was also studied *via* quantum mechanical calculations using Gaussian 09. Calculations of frontier molecular orbital HOMO (highest occupied molecular orbital) and LUMO (lowest unoccupied molecular orbital) energies and band gaps were performed in the gas phase. The structure was optimized using the B3LYP theoretical method with the 6-311g(d,p) and LANL2DZ basis sets (Fig. 9). The calculations predicted that the bandgaps between the HOMOs and LUMOs of **HJ-DNP** with arsenate and PPi were found to be 1.49 eV and 1.39 eV, respectively (Fig. S20†). These results confirm a decrease in energy compared to free **HJ-DNP**, which validates the spectral shifts in the experimental absorption spectra.

The binding energies (ΔE) for probe **HJ-DNP**–arsenate and probe **HJ-DNP**–PPi complexes were computed *via* calculating the differences between the energies of the isolated receptor and anions and their complexes (Table 1). The calculated binding energies for the corresponding arsenate and PPi complexes are –351 and –228 kJ mol^{-1}, respectively, revealing the higher affinity of **HJ-DNP** for arsenate than PPi. These results are well in line with the experimental results.

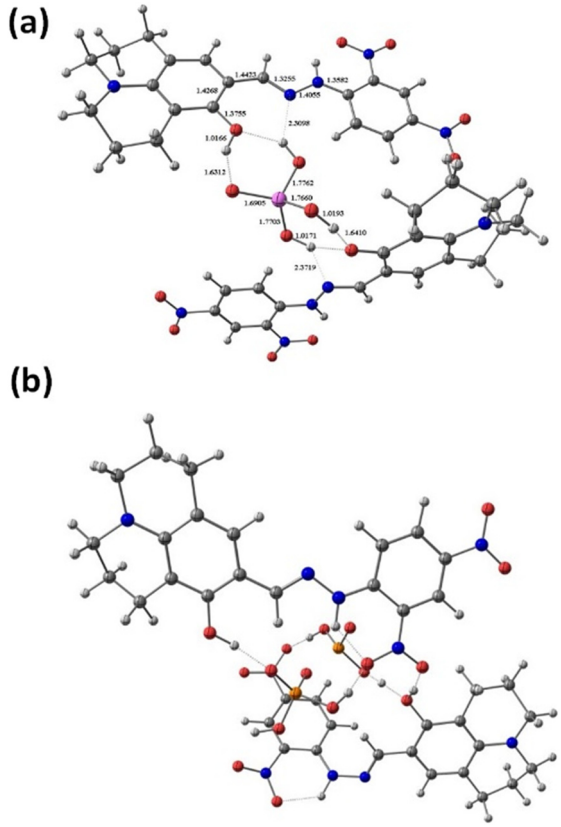

Fig. 9 Optimized structures of (a) **HJ-DNP**–arsenate and (b) **HJ-DNP**–PPi at the B3LYP/LANL2DZ level of theory.

Table 1 Computed total energies and binding energies (ΔE_{bind}) of **HJ-DNP**–anion complexes obtained at the B3LYP/LANL2DZ level

Compound	Total energy (a.u.)			ΔE_{bind} (kJ mol^{-1})
	HJ-DNP–anion	**HJ-DNP** only	Anion only	
Arsenate	−3077.23271	−1384.52253	−308.05396	−351
PPi	−3310.95527	−1384.52253	−541.82046	−228

The primary source of binding energy in the **HJ-DNP**–arsenate and **HJ-DNP**–PPi complexes was hydrogen bonding between –OH, –NH, and –NO_2 groups present in the framework of **HJ-DNP** and the anions.

2.5. pH-Dependent studies

The effects of pH on the sensing behaviour of the probe **HJ-DNP** were studied based on changes in the UV-vis spectrum. Three different pH levels, pH 5.0, 7.0, and 9.0, were chosen in order to explore acidic, neutral, and basic pH conditions. The experiments were performed using acetate buffer, water, and borax buffer to maintain the respective pH levels. From a comparative table of LOD values (Table S3†), it is evident that the probe **HJ-DNP** can efficiently detect analytes only at neutral pH (Fig. S21 and S22†). At acidic pH (pH = 5), changes in UV-vis absorbance and colour are very minimal or negligible, so LOD calculations are not feasible. However, at pH 9.0, in basic medium, only Cr^{3+} effectively binds with **HJ-DNP**, as the probe deprotonates in a basic medium and binding sites are not available for the binding of anions such as arsenate and PPi. Thus, pH studies confirm that acidic pH is not suitable for the binding of analytes. However, interestingly, at basic pH the probe is selective for Cr^{3+}.

2.6. Arsenate detection in real samples

Arsenate detection was carried out using three natural water samples (groundwater, pond water, and tap water) and washed rice water (WRW). Rice is a significant contributor of inorganic arsenic in the human diets. Rice accumulates a higher amount of arsenic than any other grain crop. Arsenic-containing irrigation water can lead to long-term soil contamination with arsenic.[49,50] In soil, arsenic is present mainly as inorganic species (arsenate As(v) and arsenic As(iii)).[43,51] Therefore, we have selected a water sample obtained from rice washing. It is known that 50–60% of arsenic impurities are removed upon soaking rice in water before cooking. Arsenate-spiked water samples were used for recovery analysis. Fluorescence spectra were recorded, and the emission intensity at 522 nm was monitored. The response of **HJ-DNP** increased linearly with an increase in the arsenate concentration in spiked water.

Based on emission changes, the arsenate % recovery values were estimated, and acceptable average recovery (95.0–105%) and RSD (2.0–4.0%) values were obtained (Table 2). The recovery of arsenate from wastewater samples was statistically close to 100%. This result indicates the validation of this method for the detection of arsenate in different water samples and washed rice water. In addition, the concentration of arsenate in these samples detected *via* the proposed approach agreed well with ICP-MS experiments. These studies implied that the sensor **HJ-DNP** could be a promising tool for monitoring arsenate in water and grains like rice.

2.7. Detection of arsenate ions using sodium alginate beads

The use of alginate beads (biopolymer) as a sorbent to detect and remove arsenate from contaminated water has also been investigated. The probe **HJ-DNP** was incorporated with

Table 2 The recovery data set for different water samples spiked with $HAsO_4^{2-}$

Water sample	$HAsO_4^{2-}$ spiked (μM)	Found (μM)	Recovery %	RSD% (n = 3)
Ground	40	38.63	96.57	3.03
	80	75.67	94.58	1.86
Pond	20	20.08	100.0	2.13
	80	76.02	95.02	2.47
	100	96.08	96.08	2.58
Tap	20	19.78	98.90	3.15
	60	60.03	100.0	3.09
	100	98.08	98.08	2.36
Washed rice	80	76.79	95.98	3.91
	100	100.03	100.13	3.43

polymeric sodium alginate beads[52,53] for ready-to-use applications. **HJ-DNP**-incorporating alginate hydrogel beads (**HJ-DNP**@alginate) were prepared using distilled water *via* a well-known method described previously (see the Experimental details below).

HJ-DNP@alginate was characterized *via* scanning electron microscopy (SEM) and EDX analysis. As shown in Fig. 10A, the beads display an uneven polymer surface, indicating the incorporation of **HJ-DNP** on the surface of the polymer.[54] **HJ-DNP**@alginate was immersed in a sample of arsenate-contaminated water. An immediate change in the colour of the polymer beads from dark yellow to red confirms the detection of arsenate and its uptake by the polymer beads (Fig. 10).

SEM–EDX analysis of red-coloured **HJ-DNP**@alginate confirmed the detection and adsorption of arsenate ions from water samples (Fig. 10B). Arsenic peaks were observed in the SEM–EDX spectra only after arsenate adsorption by the alginate beads. This phenomenon shows the effective adsorption of arsenate on the surface of **HJ-DNP**@alginate. Thus, these experiments confirm the advantage of using **HJ-DNP**@alginate for the detection of μM-levels of arsenate in water.

2.8. Multianalyte detection based on the CIE chromaticity diagram

The CIE 1931 chromaticity parameters (x, y) from the luminescence data of **HJ-DNP**, **HJ-DNP** with Cr^{3+}, and **HJ-DNP** with anions were calculated, and the chromaticity diagram was plotted.[55–57] Fig. 11 depicts the changes in the CIE coordinates in response to various analytes. The CIE diagram shows the luminescence of probe **HJ-DNP** in the presence of arsenate, PPi, and Cr^{3+}. The probe **HJ-DNP** (0.36, 0.35) lies in the centre of the red colour space, showing no specific fluorescence. But with analytes, this changes and moves to different regions.

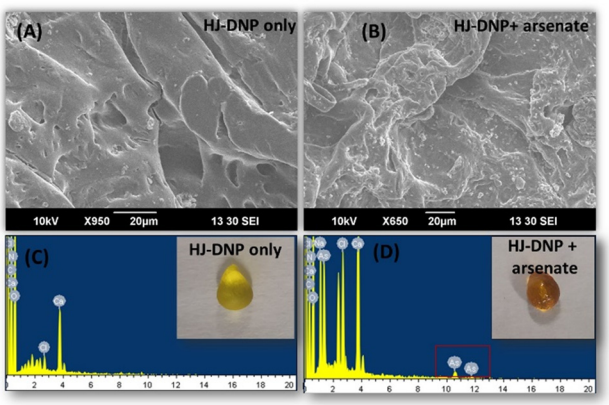

Fig. 10 Scanning electron microscopy images of (A) the probe **HJ-DNP** and (B) **HJ-DNP** that had adsorbed arsenate on the surface of sodium alginate hydrogel beads. (C) The SEM–EDX profile of **HJ-DNP** on sodium alginate hydrogel beads (the inset shows the yellow-coloured bead). (D) The SEM–EDX profile of **HJ-DNP** with arsenate on sodium alginate hydrogel beads (the inset shows the orange-coloured bead).

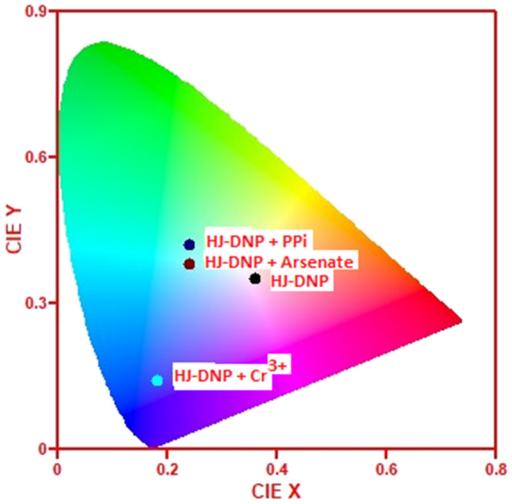

Fig. 11 The CIE chromaticity diagram of the probe **HJ-DNP** with the analytes pyrophosphate (PPi), arsenate, and Cr^{3+}.

In the presence of arsenate, the probe displayed chromaticity in the blue region, and this moved towards the green region upon the addition of PPi. Again, the chromaticity shifted towards the blue-purple region in the presence of Cr^{3+}, unlike PPi and arsenate. Therefore, it is evident that the probe **HJ-DNP** could be used to detect and distinguish between the three analytes of Cr^{3+}, arsenate, and PPi.

3. Experimental section

General information and materials

All the chemicals used were purchased from commercial sources and used without further purification. 8-Hydroxyjulolidine-9-carboxaldehyde was purchased from TCI Chemicals. 2,4-Dinitrophenylhydrazine, tetrabutylammonium salts of different anions (such as Cl^-, I^-, Br^-, CH_3COO^-, PO_4^{3-}, NO_3^-, F^-, OH^-, $P_2O_7^{4-}$, and HSO_4^-), and the sodium salt of arsenate ($HAsO4_2^-$) were purchased from Sigma-Aldrich. Perchlorate salts of various metal ions, such as Mn^{2+}, Mg^{2+}, Ca^{2+}, Na^+, Fe^{2+}, Fe^{3+}, Cu^{2+}, Ni^{2+}, Al^{3+}, Co^{3+}, Cr^{3+}, Hg^{2+}, and Ag^+, were purchased from Sigma-Aldrich. Solvents were obtained from Loba Chemie and S. D. fine chemical and were used following further purification *via* distillation. ^{1}H-NMR spectra were recorded using a Bruker Avance (II) 600 MHz NMR instrument with TMS as an internal standard. Mass spectra were obtained using a XEVO G2-XS QTOF (LC-MS) spectrometer. An Agilent Technologies Cary Eclipse fluorescence spectrophotometer was used to obtain fluorescence spectra. Absorption spectra were recorded using an Agilent Technology UV-vis spectrophotometer, using quartz cells with a path length of 1.0 cm.

Synthesis of the probe HJ-DNP

250 mg of 8-hydroxyjulolidine-9-carboxaldehyde (1.15 mmol) and 228 mg of 2,4-dinitrophenylhydrazine (1.15 mmol) were dissolved in distilled methanol (30 mL) and allowed to react with each other for 24 h under N_2 to form an orange precipitate. The reaction was then stopped, and the precipitate was filtered and washed with cold methanol. The solid product was further precipitated in a warm methanol–ethanol mixture and collected as a dark orange-coloured solid, yielding the pure compound **HJ-DNP**. Yield = 79.6%. ^{1}H-NMR (600 MHz, DMSO-d_6): δ (ppm) 15.13 (s, 1H), 9.89 (s, 1H), 9.33 (s, 1H), 8.31 (d, J = 6 Hz, 1H), 8.04 (d, J = 12 Hz, 2H), 7.89 (d, J = 6 Hz, 2H), 7.59 (m, 4H), 7.24 (d, J = 12 Hz, 1H), 7.08 (d, J = 12 Hz, 1H), 6.97 (d, J = 6 Hz, 1H). ^{13}C-NMR (150 MHz, DMSO-d_6): δ (ppm) 167.50, 160.04, 152.06, 148.45, 143.67, 142.25, 131.56, 130.59, 129.39, 128.77, 127.38, 125.35, 122.09, 119.32, 118.42, 116.04, 115.83. MS-ES (m/z) $C_{19}H_{19}N_5O_5$: calculated, 397.14; found, 398.8412.

Binding constant determination

The binding constant (K_a) values of **HJ-DNP** with different analytes in DMSO–water (80 : 20) were determined based on Hill plots, using the formula K_a = 1/slope. The slope was obtained *via* the linear fitting of a plot of the emission or intensity *vs.* the concentration of analyte.

The calculation of the limit of detection (LOD)

LOD was calculated using the equation (3.3σ/slope), where σ is the standard deviation of the λ_{max} intensity value of the blank probe **HJ-DNP**. The slope was obtained *via* the linear fitting of a plot of intensity *vs.* the analyte concentration.

DFT studies

All calculations were carried out using the Gaussian 09 program package.[58] The geometries of all compounds were fully optimized and investigated using the density functional theory method (B3LYP) with the 6-311g(d,p) and LANL2DZ basis sets.

Conclusions

In summary, a new fluorescent and colorimetric sensor, **HJ-DNP**, was developed to detect the multiple analytes of Cr^{3+}, arsenate, and PPi ions in aqueous solution. The probe **HJ-DNP** displayed aggregation-induced emission (AIE) behaviour at 585 nm, with a 10-fold increase in the emission intensity upon increasing the proportion of water in DMSO. The ESIPT mechanism of the probe **HJ-DNP** was explored *via* DFT calculations and studying the optimized geometries of **HJ-DNP** in both keto and enol forms. The probe **HJ-DNP** could preferentially detect Cr^{3+} ions over various metal ions *via* the CHEF mechanism with a turn-on response. The LOD towards Cr^{3+} ions was calculated to be 3.9 μM. The probe **HJ-DNP** was also used to detect Cr^{3+} in the food product tomatoes. Among various anions/oxyanions, **HJ-DNP** could detect arsenate and pyrophosphate ions *via* a colour change from pale orange to red. Also, there were changes in the emission spectra. The LOD values toward arsenate and PPi were calculated to be as low as 3.9 μM and 0.19 mM, respectively. The different emission behaviour of **HJ-DNP** in the presence of PPi and arsenate enabled us to distinguish between these ions in water. The probe **HJ-DNP** is also incorporated with sodium alginate polymer beads for ready-to-use detection and arsenate removal from water. Lifetime measurements and ^{1}H-NMR titration studies were performed to confirm the proposed binding modes and mechanisms. Furthermore, arsenate detection was carried out in real-life water samples, such as groundwater, pond water, tap water, and rice washing water. It is also evident from the CIE chromaticity plot that the probe **HJ-DNP** can act as an efficient probe for detecting the multiple analytes of Cr^{3+}, arsenate, and PPi.

Author contributions

Srushti Gadiyaram: methodology, investigation, validation. Amrita Ghosh: investigation, validation. Vikas D. Ghule: investigation, validation. D. Amilan Jose: conceptualization, methodology, resources, supervision, funding acquisition, writing: review and editing.

Conflicts of interest

The authors declare no conflicts of interest.

Acknowledgements

DAJ thanks DST-SERB, Core Research Grant no. EMR/2017/004085 for financial help.

Notes and references

1 D. Wu, A. C. Sedgwick, T. Gunnlaugsson, E. U. Akkaya, J. Yoon and T. D. James, Fluorescent chemosensors: the past, present and future, *Chem. Soc. Rev.*, 2017, **46**, 7105–7123.
2 K. P. Carter, A. M. Young and A. E. Palmer, Fluorescent Sensors for Measuring Metal Ions in Living Systems, *Chem. Rev.*, 2014, **114**, 4564–4601.
3 D. Cao, Z. Liu, P. Verwilst, S. Koo, P. Jangjili, J. S. Kim and W. Lin, Coumarin-Based Small-Molecule Fluorescent Chemosensors, *Chem. Rev.*, 2019, **119**, 10403–10519.
4 T. L. Mako, J. M. Racicot and M. Levine, Supramolecular Luminescent Sensors, *Chem. Rev.*, 2019, **119**, 322–477.
5 A. C. Sedgwick, L. Wu, H.-H. Han, S. D. Bull, X.-P. He, T. D. James, J. L. Sessler, B. Z. Tang, H. Tian and J. Yoon, Excited-state intramolecular proton-transfer (ESIPT) based fluorescence sensors and imaging agents, *Chem. Soc. Rev.*, 2018, **47**, 8842–8880.
6 J. Mei, N. L. C. Leung, R. T. K. Kwok, J. W. Y. Lam and B. Z. Tang, Aggregation-Induced Emission: Together We Shine, United We Soar!, *Chem. Rev.*, 2015, **115**, 11718–11940.
7 Y. Chen, J. W. Y. Lam, R. T. K. Kwok, B. Liu and B. Z. Tang, Aggregation-induced emission: fundamental

understanding and future developments, *Mater. Horiz.*, 2019, **6**, 428–433.

8 J. Luo, Z. Xie, J. W. Y. Lam, L. Cheng, H. Chen, C. Qiu, H. S. Kwok, X. Zhan, Y. Liu, D. Zhu and B. Z. Tang, Aggregation-induced emission of 1-methyl-1,2,3,4,5-pentaphenylsilole, *Chem. Commun.*, 2001, 1740–1741.

9 J. Zhao, S. Ji, Y. Chen, H. Guo and P. Yang, Excited state intramolecular proton transfer (ESIPT): from principal photophysics to the development of new chromophores and applications in fluorescent molecular probes and luminescent materials, *Phys. Chem. Chem. Phys.*, 2012, **14**, 8803–8817.

10 J. E. Kwon and S. Y. Park, Advanced Organic Optoelectronic Materials: Harnessing Excited-State Intramolecular Proton Transfer (ESIPT) Process, *Adv. Mater.*, 2011, **23**, 3615–3642.

11 V. Bhardwaj, L. Hindocha, S. K. Ashok Kumar and S. K. Sahoo, An aggregation-induced emissive pyridoxal derived tetradentate Schiff base for the fluorescence turn-off sensing of copper(ii) in an aqueous medium, *New J. Chem.*, 2022, **46**, 3248–3257.

12 Z. Zhou, Y. Li, W. Su, B. Gu, H. Xu, C. Wu, P. Yin, H. Li and Y. Zhang, A dual-signal colorimetric and near-infrared fluorescence probe for the detection of exogenous and endogenous hydrogen peroxide in living cells, *Sens. Actuators, B*, 2019, **280**, 120–128.

13 J. L. Kolanowski, F. Liu and E. J. New, Fluorescent probes for the simultaneous detection of multiple analytes in biology, *Chem. Soc. Rev.*, 2018, **47**, 195–208.

14 M. Chhatwal, A. Kumar, V. Singh, R. D. Gupta and S. K. Awasthi, Addressing of multiple-metal ions on a single platform, *Coord. Chem. Rev.*, 2015, **292**, 30–55.

15 Y. Tu, Y. Yu, D. Xiao, J. Liu, Z. Zhao, Z. Liu, J. W. Y. Lam and B. Z. Tang, An Intelligent AIEgen with Nonmonotonic Multiresponses to Multistimuli, *Adv. Sci.*, 2020, **7**, 2001845.

16 V. Kumar, H. Rana, G. Raviraju, P. Garg, A. Baghel and A. K. Gupta, Chromogenic and fluorogenic multianalyte detection with a tuned receptor: refining selectivity for toxic anions and nerve agents, *RSC Adv.*, 2016, **6**, 59648–59656.

17 R. Kaushik, R. Sakla, N. Kumar, A. Ghosh, V. D. Ghule and D. A. Jose, Multianalytes Sensing Probe: Fluorescent Moisture Detection, Smartphone Assisted Colorimetric Phosgene recognition and Colorimetric Discrimination of Cu2+and Fe3+ ions, *Sens. Actuators, B*, 2021, **328**, 129026.

18 F. Ali, S. Saha, A. Maity, N. Taye, M. K. Si, E. Suresh, B. Ganguly, S. Chattopadhyay and A. Das, Specific Reagent for Cr(III): Imaging Cellular Uptake of Cr(III) in Hct116 Cells and Theoretical Rationalization, *J. Phys. Chem. B*, 2015, **119**, 13018–13026.

19 P. Mahato, S. Saha, E. Suresh, R. Di Liddo, P. P. Parnigotto, M. T. Conconi, M. K. Kesharwani, B. Ganguly and A. Das, Ratiometric Detection of Cr3+ and Hg2+ by a Naphthalimide-Rhodamine Based Fluorescent Probe, *Inorg. Chem.*, 2012, **51**, 1769–1777.

20 V. Raju, R. Selva Kumar, S. K. Ashok Kumar, Y. Tharakeswar and S. K. Sahoo, Development of highly selective chemosensor for chomium(III) estimation in aqueous environment, *Inorg. Chem. Commun.*, 2019, **101**, 74–80.

21 V. K. Gupta, N. Mergu and A. K. Singh, Rhodamine-derived highly sensitive and selective colorimetric and off–on optical chemosensors for Cr3+, *Sens. Actuators, B*, 2015, **220**, 420–432.

22 S. Dutta, S. Let, M. M. Shirolkar, A. V. Desai, P. Samanta, S. Fajal, Y. D. More and S. K. Ghosh, A luminescent cationic MOF for bimodal recognition of chromium and arsenic based oxo-anions in water, *Dalton Trans.*, 2021, **50**, 10133–10141.

23 Q.-Q. He, S.-L. Yao, T.-F. Zheng, H. Xu, S.-J. Liu, J.-L. Chen, N. Li and H.-R. Wen, A multi-responsive luminescent sensor based on a stable Eu(III) metal-organic framework for sensing Fe3+, MnO4-, and Cr2O72- in aqueous solutions, *CrystEngComm*, 2022, **24**, 1041–1048.

24 T. Hu, L. Wang, J. Li, Y. Zhao, J. Cheng, W. Li, Z. Chang and C. Sun, A new fluorescent sensor L based on fluorene-naphthalene Schiff base for recognition of Al3+ and Cr3+, *Inorg. Chim. Acta*, 2021, **524**, 120421.

25 M.-J. Tsai, K.-S. Liao and J.-Y. Wu, A Water-Stable 2-Fold Interpenetrating cds Net as a Bifunctional Fluorescence-Responsive Sensor for Selective Detection of Cr(III) and Cr(VI) Ions, *Nanomaterials*, 2022, **12**, 158.

26 C. Wang, S. Ma, L. Pan, W. Wu, Y. Wei and J. Ou, Cyclized conjugated microporous polymer-coated silica nanospheres as fluorescent sensors for iron (III) and chromium (III), *Chem. Eng. J.*, 2022, **435**, 134368.

27 X. Wang, Y. Zhang, Z. Shi, T. Lu, Q. Wang and B. Li, Multifunctional Zr-MOF Based on Bisimidazole Tetracarboxylic Acid for pH Sensing and Photoreduction of Cr(VI), *ACS Appl. Mater. Interfaces*, 2021, **13**, 54217–54226.

28 H. Zhao, J. Zhang, X. Lin, H. Li and Q. Pan, Synthesis of 4-dimethylaminobenzyl chrysin ester-Zn fluorescent chemical sensor for the determination of Cr(VI) in water, *Luminescence*, 2022, **37**, 72–81.

29 X. Zheng, S. Ren, L. Wang, Q. Gai, Q. Dong and W. Liu, Controllable functionalization of carbon dots as fluorescent sensors for independent Cr(VI), Fe(III) and Cu(II) ions detection, *J. Photochem. Photobiol., A*, 2021, **417**, 113359.

30 N. Mekjinda, S. Phunnarungsi, V. Ruangpornvisuti, R. J. Ritchie, I. Hamachi, A. Ojida and J. Wongkongkatep, Masking Phosphate with Rare-Earth Elements Enables Selective Detection of Arsenate by Dipycolylamine-ZnII Chemosensor, *Sci. Rep.*, 2020, **10**, 2656.

31 J. Ma, M. K. Sengupta, D. Yuan and P. K. Dasgupta, Speciation and detection of arsenic in aqueous samples: A review of recent progress in non-atomic spectrometric methods, *Anal. Chim. Acta*, 2014, **831**, 1–23.

32 D. Banik, S. K. Manna and A. K. Mahapatra, Recent development of chromogenic and fluorogenic chemosensors for the detection of arsenic species: Environmental and biological applications, *Spectrochim. Acta, Part A*, 2021, **246**, 119047.

33 W. Paisuwan, T. Lertpiriyasakulkit, V. Ruangpornvisuti, M. Sukwattanasinitt and A. Ajavakom, 8-Hydroxyjulolidine

aldimine as a fluorescent sensor for the dual detection of Al3+ and Mg2+, *Sens. Bio-Sens. Res.*, 2020, **29**, 100358.

34 J. Du, B. Zhao, W. Kan, H. Yin, T. Song, L. Wang, L. Sun, X. Wang, G. Yin and J. Wang, A phenanthrene[9,10-d] imidazole-phenol-based fluorescent probe combining ESIPT and AIE for the "turn-on" detection of Cu2+ with green-emission and improved Stokes' shift, and its application, *New J. Chem.*, 2021, **45**, 15415–15422.

35 H. Liu, X. Wang, Y. Xiang and A. Tong, Fluorescence turn-on detection of cysteine over homocysteine and glutathione based on "ESIPT" and "AIE", *Anal. Methods*, 2015, **7**, 5028–5033.

36 Y. Chen, T. Wei, Z. Zhang, T. Chen, J. Li, J. Qiang, J. Lv, F. Wang and X. Chen, A Benzothiazole-Based Fluorescent Probe for Ratiometric Detection of Al3+ in Aqueous Medium and Living Cells, *Ind. Eng. Chem. Res.*, 2017, **56**, 12267–12275.

37 J.-C. Qin, B.-D. Wang, Z.-Y. Yang and K.-C. Yu, A ratiometric fluorescent chemosensor for Zn2+ in aqueous solution through an ESIPT coupled AIE process, *Sens. Actuators, B*, 2016, **224**, 892–898.

38 X. Wan, H. Liu, S. Yao, T. Liu and Y. Yao, A stimuli-responsive nanogel-based sensitive and selective fluorescent sensor for Cr(3+) with thermo-induced tunable detection sensitivity, *Macromol. Rapid Commun.*, 2013, **35**, 323–329.

39 B. Janani, K. M. Alarjani, L. L. Raju, A. M. Thomas, A. Das and S. S. Khan, A potent multifunctional Ag/Co-polyvinylpyrrolidone nanocomposite for enhanced detection of Cr(III) from environmental samples and its photocatalytic and antibacterial applications, *Spectrochim. Acta, Part A*, 2020, **243**, 118766.

40 O. O. Olayinka and A. R. Ipeaiyeda, Chromium and Lead Concentrations in Tomatoes (Solanum Lycopersicum) and Red Peppers (Capsicum Frutescens) Cultivated in Roadside Farmland around High Traffic Density Area of Ibadan, Nigeria, *Soil Sediment Contam.*, 2011, **20**, 1–11.

41 D. Romero-Estévez, G. S. Yánez-Jácome, K. Simbaña-Farinango, P. Y. Vélez-Terreros and H. Navarrete, Determination of cadmium and lead in tomato (Solanum lycopersicum) and lettuce (Lactuca sativa) consumed in Quito, Ecuador, *Toxicol. Rep.*, 2020, **7**, 893–899.

42 S. Dey, S. Sarkar, D. Maity and P. Roy, Rhodamine based chemosensor for trivalent cations: Synthesis, spectral properties, secondary complex as sensor for arsenate and molecular logic gates, *Sens. Actuators, B*, 2017, **246**, 518–534.

43 A. S. M. Islam, R. Alam, A. Katarkar, K. Chaudhuri and M. Ali, Di-oxime based selective fluorescent probe for arsenate and arsenite ions in a purely aqueous medium with living cell imaging applications and H-bonding induced microstructure formation, *Analyst*, 2015, **140**, 2979–2983.

44 S. Nandi, A. Sahana, B. Sarkar, S. K. Mukhopadhyay and D. Das, Pyridine Based Fluorescence Probe: Simultaneous Detection and Removal of Arsenate from Real Samples with Living Cell Imaging Properties, *J. Fluoresc.*, 2015, **25**, 1191–1201.

45 L. Tong, X. Wang, W. Gao, Z. Liu, Z. Chen, G. Cheng, W. Cao, M. Sui and B. Tang, CeO2 Nanowire-BODIPY-Adenosine Triphosphate Fluorescent Sensing Platform for Highly Specific and Sensitive Detection of Arsenate, *Anal. Chem.*, 2018, **90**, 14507–14513.

46 S. Lee, K. K. Y. Yuen, K. A. Jolliffe and J. Yoon, Fluorescent and colorimetric chemosensors for pyrophosphate, *Chem. Soc. Rev.*, 2015, **44**, 1749–1762.

47 J. Wongkongkatep, A. Ojida and I. Hamachi, Fluorescence Sensing of Inorganic Phosphate and Pyrophosphate Using Small Molecular Sensors and Their Applications, *Top. Curr. Chem.*, 2017, **375**, 30.

48 S. Anbu, A. Paul, G. J. Stasiuk and A. J. L. Pombeiro, Recent developments in molecular sensor designs for inorganic pyrophosphate detection and biological imaging, *Coord. Chem. Rev.*, 2021, **431**, 213744.

49 K. Pramanik, P. Sarkar and D. Bhattacharyay, 3-Mercapto-propanoic acid modified cellulose filter paper for quick removal of arsenate from drinking water, *Int. J. Biol. Macromol.*, 2019, **122**, 185–194.

50 J. Das and P. Sarkar, A new dipstick colorimetric sensor for detection of arsenate in drinking water, *Environ. Sci.: Water Res. Technol.*, 2016, **2**, 693–704.

51 B. Yuan, J. Qu and Q. Lin, Fluorimetric Determination of Arsenite and Arsenate in Water Using Fluorescein and Iodine, *Int. J. Environ. Anal. Chem.*, 2002, **82**, 31–36.

52 I. Jung, H. B. Seo, J.-E. Lee, B. Chan Kim and M. B. Gu, A dip-stick type biosensor using bioluminescent bacteria encapsulated in color-coded alginate microbeads for detection of water toxicity, *Analyst*, 2014, **139**, 4696–4701.

53 H. Zhu, Q. Zhang and S. Zhu, Alginate Hydrogel: A Shapeable and Versatile Platform for in Situ Preparation of Metal–Organic Framework–Polymer Composites, *ACS Appl. Mater. Interfaces*, 2016, **8**, 17395–17401.

54 P. Kumar and D. A. Jose, Naked eye detection of moisture in organic solvents and development of alginate polymer beads and test cassettes as a portable kit, *Anal. Chim. Acta*, 2020, **1136**, 178–186.

55 F. Arshad and M. P. Sk, Aggregation-induced red shift in N,S-doped chiral carbon dot emissions for moisture sensing, *New J. Chem.*, 2019, **43**, 13240–13248.

56 P. Kumar, S. Gadiyaram and D. A. Jose, Simple Iron(III) Complex Based Highly Sensitive Fluorescent Off-On Sensor for the Detection of Trace Amount of Water in Organic Solvents and Edible Oilseeds, *ChemistrySelect*, 2020, **5**, 10648–10655.

57 J.-S. Kim, H.-B. Oh, A. H. Kim, J.-S. Kim, E.-S. Lee, J.-Y. Baek, K. S. Lee, S.-C. Chung and J.-H. Jun, A study on detection of glucose concentration using changes in color coordinates, *Bioengineered*, 2017, **8**, 99–104.

58 M. J. Frisch, G. W. Trucks, H. B. Schlegel, G. E. Scuseria, M. A. Robb, J. R. Cheeseman, G. Scalmani, V. Barone, G. A. Petersson, H. Nakatsuji, X. Li, M. Caricato, A. V. Marenich, J. Bloino, B. G. Janesko, R. Gomperts, B. Mennucci, H. P. Hratchian, J. V. Ortiz, A. F. Izmaylov, J. L. Sonnenberg, D. Williams-Young, F. Ding, F. Lipparini, F. Egidi, J. Goings, B. Peng, A. Petrone, T. Henderson, D. Ranasinghe, V. G. Zakrzewski, J. Gao, N. Rega, G. Zheng, W. Liang, M. Hada,

M. Ehara, K. Toyota, R. Fukuda, J. Hasegawa, M. Ishida, T. Nakajima, Y. Honda, O. Kitao, H. Nakai, T. Vreven, K. Throssell, J. A. Montgomery, Jr., J. E. Peralta, F. Ogliaro, M. J. Bearpark, J. J. Heyd, E. N. Brothers, K. N. Kudin, V. N. Staroverov, T. A. Keith, R. Kobayashi, J. Normand, K. Raghavachari, A. P. Rendell, J. C. Burant, S. S. Iyengar, J. Tomasi, M. Cossi, J. M. Millam, M. Klene, C. Adamo, R. Cammi, J. W. Ochterski, R. L. Martin, K. Morokuma, O. Farkas, J. B. Foresman and D. J. Fox, *Gaussian 16 Rev. B.01*, Wallingford, CT, 2016.